ACS OMEGA

Article

Cite This: ACS Omega 2019, 4, 10702−10713

http://pubs.acs.org/journal/acsodf

Nitrogen-Doped Graphene Oxide Dots-Based "Turn-OFF" H_2O_2, Au(III), and "Turn-OFF−ON" Hg(II) Sensors as Logic Gates and Molecular Keypad Locks

Naveen Kumar Reddy Bogireddy,[†] Victor Barba,[‡] and Vivechana Agarwal*,[†]

[†]Centro de Investigación en Ingeniería y Ciencias Aplicadas, UAEM, Av. Univ. 1001, Col. Chamilpa, Cuernavaca, Morelos 62209, Mexico

[‡]Centro de Investigaciones Químicas-IICBA, Universidad Autónoma Del Estado de Morelos, Av. Universidad 1001, Col. Chamilpa, Cuernavaca, Morelos CP 62209, Mexico

Supporting Information

ABSTRACT: Fluorescent nitrogen-doped graphene oxide dots (NGODs) have been demonstrated as an on−off nanosensor for the detection of Hg^{2+}, Au^{3+}, and H_2O_2. As compared to L-cystine, where the luminescence signal recovery results from the detachment of Hg^{2+} from the NGODs, signal recovery through L-ascorbic acid (turn-off−on model) has been attributed to the reduction of Hg^{2+} to Hg^0. The sustainable recovery of the photoluminescence signal is demonstrated using common citrus fruits containing vitamin C (L-AA), suggesting a promising practical usage of this sensing system. Additionally, the sensitivity of NGOD- and AA-originated signal recovery from the Hg(II)−NGODs mixture has been successfully tested in Hg^{2+} ion-spiked tap water from three different places. Mimic devices were executed and verified on the basis of characteristic spectral changes, and the possible utility of this system in electronic security and memory element devices has also been demonstrated. Considering an easy synthesis process and excellent performance of NGODs, this investigation opens up new opportunities for preparing high-quality fluorescent NGODs to meet the requirements of many applications.

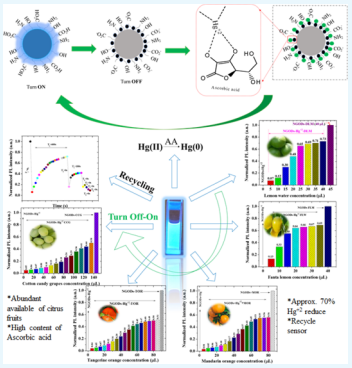

INTRODUCTION

Carbon-based fluorescent nanomaterials[1,2] have attracted attention because of their low-cost design and possible applications in different fields such as photocatalysis, optoelectronics, bioimaging,[3−6] and sensing. Some of the reported fabrication methods[7,8] are relatively complicated and accompanied with the requirement of strong acids, which could be environmentally undesirable and hazardous. Because of low toxicity, simple preparation methods, and relatively stable fluorescence signal output from carbon dots (CDs), accurate detection results have been reported for several metal ions, biomolecules,[9,10] temperature,[11] pH,[10] small organic molecules,[12] and hydrogen peroxide.[13,14]

In particular, H_2O_2 has broad industrial applications with vital significance in various processes,[13,14] such as a by-product in several enzyme-catalyzed reactions, namely, lactate, cholesterol, glucose oxidase, and so forth.[15−17] In order to obtain uninterrupted electron transfer, different types of composite materials (enzymes, polymers, dyes, metals, and metal oxides) have been proposed for H_2O_2 sensing. Among several analytical techniques (electrochemical,[18] spectrophotometry,[19] chemiluminescence,[20] and fluorimetry[21]), due to the industrial importance of H_2O_2, fluorimetry has been found to be a simple, fast, and sensitive approach for the detection of H_2O_2. Chakraborty et al.[22] reported the fluorescence quenching of C-dots (turn-off) sensor for H_2O_2 in the presence of Fe^{2+}. Recently, Chakraborty et al. and Bhunia et al.[22,23] reported H_2O_2 sensors (turn-off) from hemoglobin-derived and hemoglobin-functionalized Fe^{2+}-containing CDs. Zhang et al. and Wang et al.[24,25] have also reported sensitive detection of H_2O_2 (turn-off), using fluorescent CDs coupled with other noble metals. Song et al.[26] found H_2O_2-originated quenching of yellow fluorescence from CDs synthesized from relatively toxic *o*-phenylenediamine.

Among the metal ions, Hg^{2+} is one of the most dangerous inorganic pollutants for the environment[27−32] because of its persistence, accumulation, and high toxicity, that is, its exposure has been reported to cause several diseases (neurological, reproductive, and digestive) and even mortality.[33−37] Adverse effects of Hg^{2+} ions call for an urgent need to develop a fast and convenient detection technique.[27−37] Apart from the detection of different metal ions, such as Ag^+, Cu^{2+}, Pb^{2+}, Fe^{3+}, Cr^{6+}, Zn^{2+}, Au^{3+}, and Co^{2+}, graphene-based Hg^{2+} sensors have been studied in the last decade because of low cost, fast response, and high sensitivity. Among the recent Hg^{2+} sensors, Zhang and Chen[28] reported the specificity (fluorescence quenching; turn-off) of hydrothermally synthesized N-doped CDs using folic acid as N and C precursors with a

Received: March 28, 2019
Accepted: May 23, 2019
Published: June 20, 2019

DOI: 10.1021/acsomega.9b00858
ACS Omega 2019, 4, 10702−10713

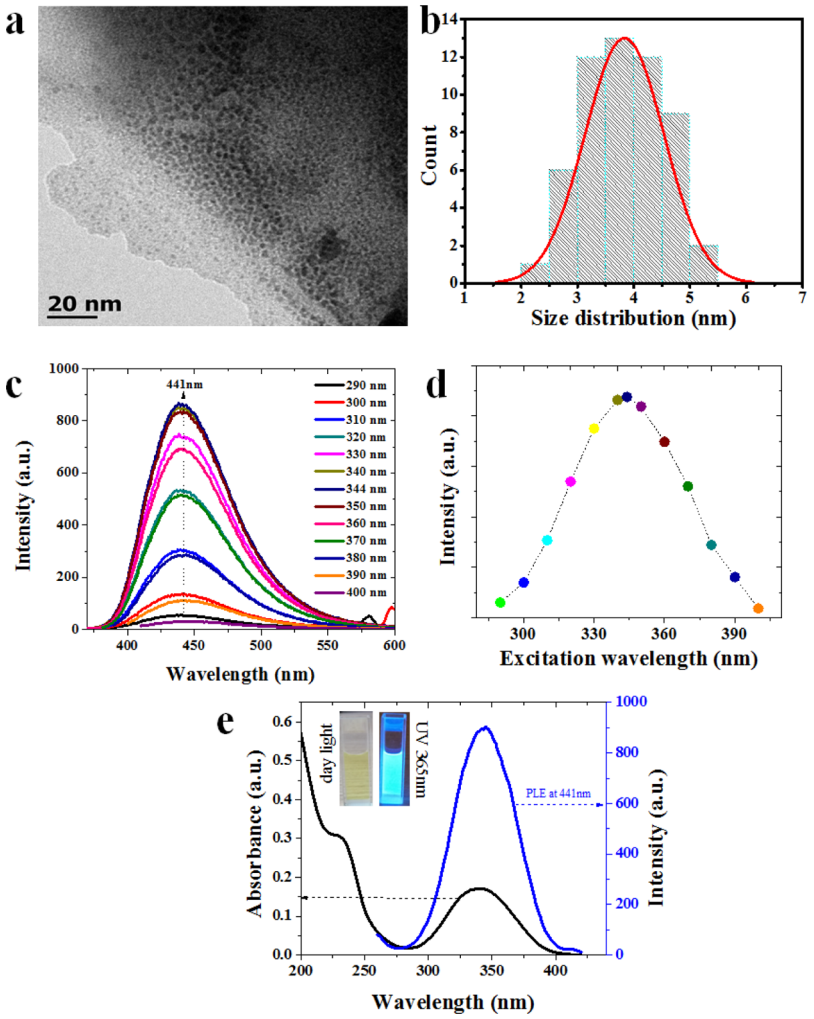

Figure 1. (a) TEM image of as-prepared NGODs and (b) size distribution analysis from (a). (c) Fluorescence emission spectra of NGODs after excitation of 290−400 nm, (d) analysis of excitation wavelength vs intensity from PL spectra, and (e) UV−visible spectra and PLE spectra of NGODs at 441 nm. The inset shows NGODs illuminated under daylight and UV light 365 nm.

detection limit of 0.23 μM. In succession, N/S co-doped (Wang et al.) CDs prepared with a simple microwave method[29] without any functionalization revealed the detection limit of 0.18 μM for Hg^{2+} and a linear signal recovery in the presence of cyanide and hydrogen sulfide (HS^-) anions. Yan et al.[30] and Zhang et al.[31] also reported the fluorescence quenching and the restoration of the signal through cysteine because of the binding preference for Hg^{2+}. Recently,[32] pineapple peel-derived CDs have been tested for reversibility of the fluorescence signal from the CD nanoprobe with alternate addition of Hg^{2+} and L-cystine (L-Cys) and additionally demonstrated for their possible utility in electronic security devices and memory element. Although, using nitrogen-doped carbon nanodots derived from various carbon sources reported the "turn-off−on" Hg^{2+} sensor using a photoluminescence (PL) recovering agent such as cyanide/hydrogen sulfide ions and cysteine, simultaneous implementation of low cost and sustainable efficient recovery from renewable/green inexpensive methods is still challenging.

Ascorbic acid (AA) and citrus fruits have recently been found effective in recovering the luminescence signal ("on-off-on" sensor) from citric acid-based CDs through the reduction of Cr^{6+}/Fe^{3+} to Cr^{3+}/Fe^{2+}. Some groups[33−36] have reported a similar "off-on" approach with AA for Fe^{3+}/Cr^{6+}-originated PL quenching of hydrothermally prepared CDs and g-C_3N_4 nanosheets, respectively. The turn-ON fluorescence in the presence of AA is explained through the redox reaction between Fe^{3+}/Cr^{6+} (reducing to Fe^{2+}/Cr^{3+}) and AA. Recently, Luo et al.[37] reported a switchable sensor based on N and S co-doped CDs to determine AA content in common fruits via signal recovery of Fe^{3+} (off) caused fluorescence quenching of CDs.

Furthermore, in spite of the proposed therapeutic use of gold, Au^{3+} is known to be toxic for human beings as the soluble salts of gold have been reported to damage kidneys, nervous system, and liver.[33] Because of the possible usefulness of fluorescent probes as an analytical tool in the field of medicine, environment, and chemistry, Gu et al.[38] and Liao et al.[39] reported CDs/NCDs as a fluorescent label-free detection of Au^{3+}.

Considering all of the above facts, in this study, citric acid and urea were chosen to hydrothermally prepare fluorescent nitrogen-doped graphene oxide dots (NGODs) for fluorimetry-based detection (turn-off) of H_2O_2, Hg^{2+}, and Au^{3+} along with the sustained recovery of the signal for Hg(II) using AA and citrus fruits. We additionally demonstrate the application of such system as a molecular keypad lock and memory device using logic gates.

DOI: 10.1021/acsomega.9b00858
ACS Omega 2019, 4, 10702−10713

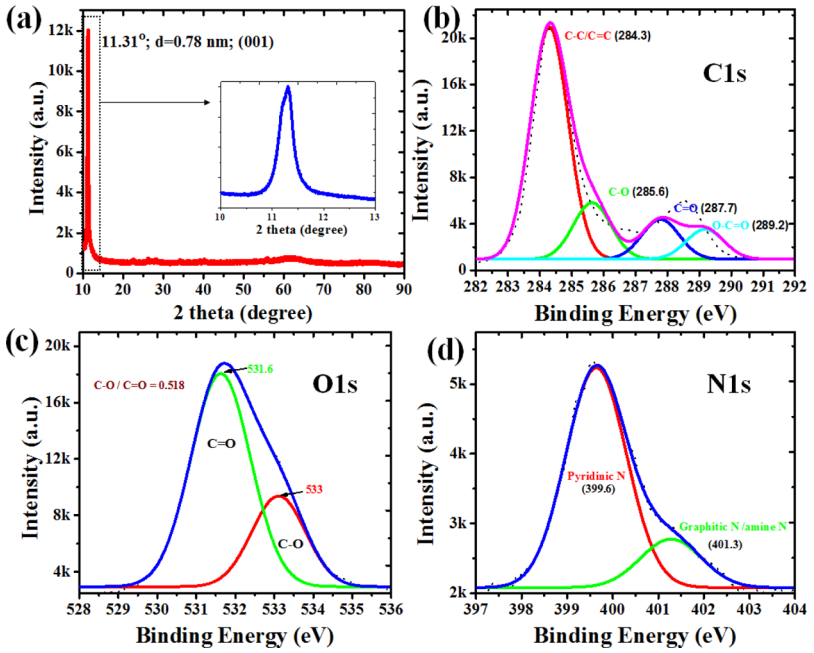

Figure 2. (a) XRD patterns of as-prepared NGODs (the inset shows enlarged view of the NGOD peak); deconvoluted XPS spectra of (b) C 1s, (c) O 1s, and (d) N 1s peaks of NGODs.

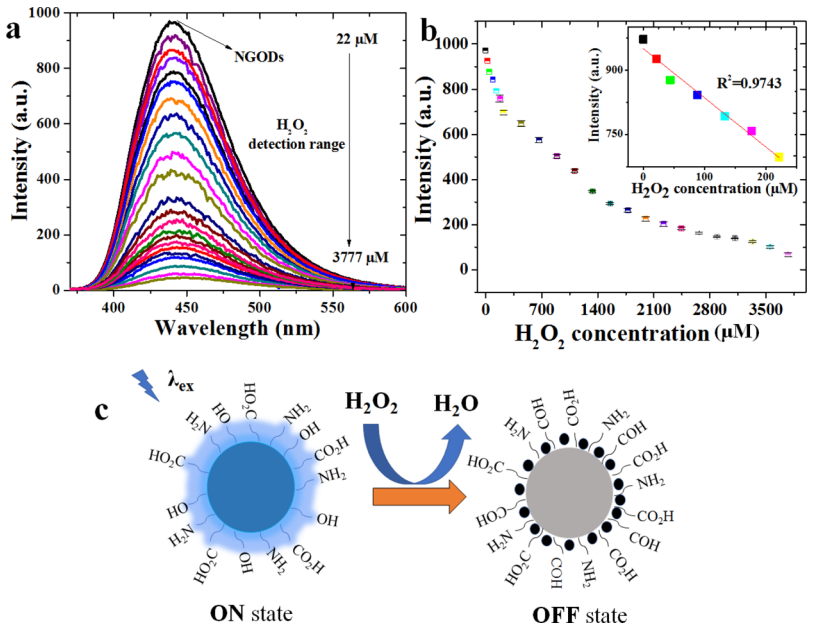

Figure 3. PL quenching pattern of NGODs in deionized water with the presence of different concentrations of H_2O_2 (a) PL vs wavelength for λ_{ex} = 344 nm, (b) PL peak intensity vs H_2O_2 concentration (the inset shows linear fit at low concentrations; R^2 = 0.974), and (c) possible quenching mechanism due to H_2O_2 adsorption on NGODs, wherein the alcohol groups are oxidized to aldehyde groups.

RESULTS AND DISCUSSION

The size distribution of as-prepared NGODs was analyzed through transmission electron microscopy (TEM, Figure 1a). The corresponding histogram (shown in Figure 1b) taken over 55 particles reveals its narrow-size distribution. The measured particle size range of 2−5.5 nm, with an average diameter of 3.8 ± 1.7 nm (Figure 1b), is in good agreement with the already reported data.[40]

Figure 1c shows the fluorescence emission intensity of NGODs at excitation wavelength range from 290 to 400 nm. It is clear that NGODs emit strong blue fluorescence at 441 nm after the irradiation (inset of Figure 1e). The PL emission intensity increases from 270 to 340 nm and then decreases in the range of 350−400 nm, indicating 344 nm as the optimal excitation wavelength for NGODs (Figure 1d). The PL excitation (PLE) spectrum measured at 441 nm (emission) (Figure 1e, blue spectra) additionally confirms the same. Moreover, the as-prepared NGODs exhibit two distinct absorption bands at around 235 nm ($\pi \rightarrow \pi^*$) and 344 nm ($n \rightarrow \pi^*$) in the UV−visible spectrum (Figure 1e, black spectra); the absorption at 344 nm (in conformity with the PLE results) is attributed to nitrogen (the doping element) as

DOI: 10.1021/acsomega.9b00858
ACS Omega 2019, 4, 10702−10713

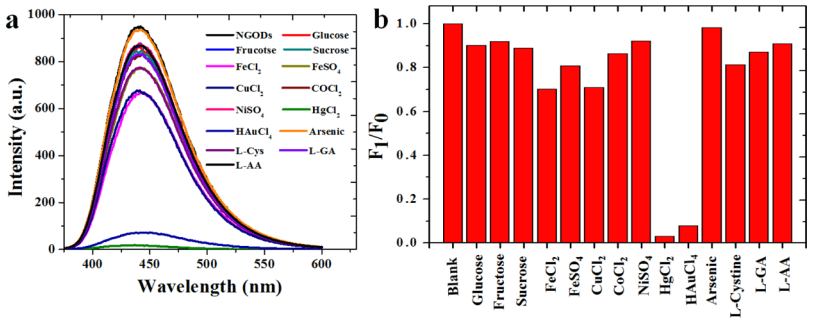

Figure 4. Selectivity of Hg^{2+} and Au^{3+} using NGODs as probes using PL spectroscopy (a) PL intensity vs wavelength at λ_{ex} = 344 nm for different metal ions at 250 μM concentration (except Au^{3+} at 300 μM) and (b) corresponding normalized graph at λ_{em} = 441 nm (F_0 = NGOD PL intensity in deionized water and F_1 = PL intensity with the metal ions). The selectivity was additionally checked with Ag^{+}, Mn^{2+}, Mg^{2+}, and Zn^{2+} (ref to Figure S3).

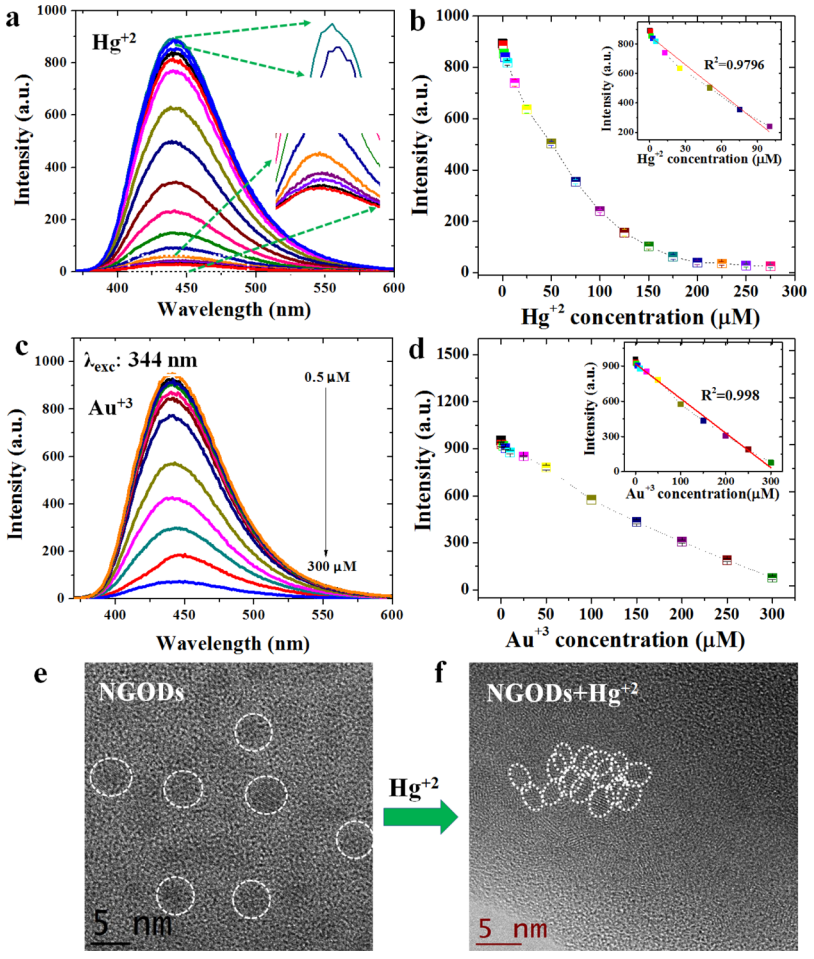

Figure 5. (a,c) PL quenching pattern of the signal intensity of NGODs in deionized water after the presence of Hg^{2+} and Au^{3+} ions, and their corresponding (b,d) concentration vs intensity analysis graphs (the inset shows linear fit of respective analysis graphs; R^2 values corresponding to Hg^{2+} and Au^{3+} are 0.954 and 0.995, respectively) and high-resolution TEM images of before (e) and after the addition of (f) agglomeration due to the formation of the Hg^{2+}−NGODs complex.

well as the strong absorption band corresponding to the graphitic structure.[41]

The X-ray diffraction (XRD) pattern of NGODs (Figure 2a) exhibits a sharp peak centered at 11.31°, which is attributed to the graphitic structure with an interlayer spacing (001) of 0.78 nm.[42−44] The survey scan of NGODs clearly shows the major peaks at 532, 400, and 285 eV, corresponding to the characteristic peaks of O 1s, N 1s, and C 1s, respectively. The occurrence of the N 1s (400 eV) peak confirms the existence of nitrogen atom in NGODs (Figure S1, Supporting Information). Furthermore, the X-ray photoelectron spectroscopy (XPS) peaks of C 1s, O 1s, and N 1s are deconvoluted to understand the chemical species present in NGODs. After deconvolution of C 1s peak of NGODs, C−C/C═C (284.3 eV), C−O (285.6 eV), C═O (287.7 eV), and O−C═O (289.2 eV) are observed (Figure 2b), revealing the existence of carbonyl and carboxyl functional groups on the surface of NGODs. Additionally, the contribution of C−N (286.5 eV)

DOI: 10.1021/acsomega.9b00858
ACS Omega 2019, 4, 10702−10713

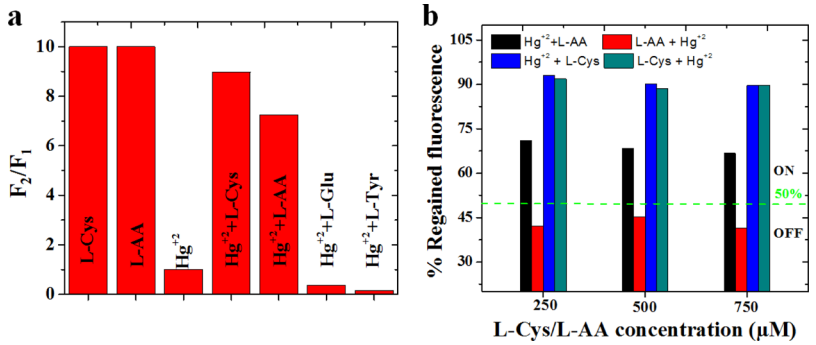

Figure 6. (a) Comparison of PL recovery: PL intensity ratio before and after the addition of 100 μM of L-AA, L-Cys, L-Glu, and L-Tyr (F_1 and F_2 correspond to PL intensities before and after the addition of the PL recovering agents, respectively) and (b) % regained PL at three different concentrations of AA and cystine.

confirms the successful incorporation of N atoms onto the NGOD structure.

Figure 2c,d showing the deconvoluted O 1s (531.6 and 533.0 eV assigned as C═O and C−O, respectively) and N 1s peaks (pyridinic N at 399.6 eV and graphitic N/amine N at 401.3 eV) of NGODs also reveals similar results. Hence, XPS results confirm the presence of N as well as oxygen-containing functional groups in NGODs. Additionally, the Fourier transform infrared (FTIR) spectrum of NGODs, shown as Figure S2 (Supporting Information), exhibiting a strong peak at 3320 cm^{-1}, designated to O−H group (stretching vibration), is in good agreement with the XPS observation with respect to the O 1s peak. The presence of hydroxyl groups on the surface suggests good hydrophilic property of NGODs. Other bands located at 2343 and 1644 cm^{-1} in the NGOD-based materials correspond to the N−H bond (stretching vibration) and C═C bond (bending vibration), respectively, of graphene.[45]

Because of the sensitivity of NGOD's PL properties, they have been investigated for H_2O_2 sensing. Figure 3a shows the PL spectra (λ_{ex} = 344 nm and λ_{em} = 441 nm) obtained for NGODs in aqueous solution with the addition of H_2O_2 in the concentration range of 22−3777 μM. As expected, the PL intensity of NGODs decreases with increasing H_2O_2 concentration, for example, with $[H_2O_2] = 3.7 \times 10^{-3}$ M, the PL from the NGOD solution was quenched by more than 90%. Figure 3b displays the concentration of H_2O_2 versus PL intensity at 441 nm. A good linear correlation (R^2 = 0.974) is shown under low concentrations ranging from 0 to 225 μM with 0.2 μM as a limit of detection (LOD) at a signal-to-noise ratio of 3. The possible quenching mechanism after the adsorption of H_2O_2 on NGODs has been attributed to the electron transfer. In fact, it is well known that organic groups such as alcohols can be oxidized to aldehydes or carboxylic acids by the presence of H_2O_2 which is reduced to H_2O[13] and hence modify the chemical environment around NGODs leading to the change of the PL properties of the nanoprobes. Herein, the PL reduction rate depends mainly on the adsorption of H_2O_2 at the surface of NGODs, reducing the electron-transfer process.

The addition of different Hg^{2+}/Au^{3+} concentrations to NGODs (Figures 4 and 5a,c) results in a drastic decrement in the PL signal intensity, implying an electron transfer between NGODs and Hg^{2+}/Au^{3+}. The fluorescence spectroscopic changes indicate that the Hg^{2+}/Au^{3+} ions coordinate with different functional groups (i.e., amine, hydroxyl, and carboxyl) present on the surface of NGODs because of the electron donor character of nitrogen (N) and oxygen (O) atoms. Hence, the coordination between functional groups on the surface favored and facilitated the electron transfer between NGODs and Hg^{2+}/Au^{3+}.[46] In other words, the proposed quenching mechanism suggests the involvement of Hg^{2+}/Au^{3+} ions as efficient electron acceptors or holes giving rise to the initiation of nonradiative electron transfer. The electrons in the excited state of NGODs can transfer to the unfilled orbitals (6p/6d) of Hg^{2+}/Au^{3+}, leading to significant quenching in the PL signal. This observation establishes NGODs as a potential candidate for the turn-off Hg^{2+}/Au^{3+} sensor. For Hg^{2+} and Au^{3+}, turn-off sensing shows a good linear correlation with R^2 as 0.954 and 0.995, respectively, under concentrations ranging from 0 to 275 μM and 0 to 300 μM with LOD to be 0.2 μM for Hg^{2+} and 0.25 μM for Au^{3+} at a signal-to-noise ratio of 3 (Figure 5b,d). The TEM images (Figure 5e,f) illustrate the agglomeration of NGODs after adding Hg^{2+} (250 μM). The added Hg^{2+} coordinated with the functional groups around the NGODs and led to an increase in the size of the complex (several metal ions aggregated numerous NGODs) with respect to the original NGODs (ref to Figure 1a).

The sensing system NGODs−Hg^{2+} can be modified by the addition of small organic molecules.[47] Although the recovery of the PL signal from the NGODs−Hg^{2+}/Au^{3+} complex was tested with various compounds, such as glucose (Glu), L-tyrosin (L-Tyr), L-Cys, and L-AA (Figure 6a), efficient recovery is observed only for L-AA and L-Cys case. For instance, the PL of NGODs was recovered with an equimolar solution of AA in the NGODs−Hg^{2+} system (Figure 6b). Nevertheless, it was observed that the PL intensity at 441 nm fails to change with the addition of only L-AA to the NGOD solution, indicating that L-AA did not affect the emission. The results indicate that PL recovery of NGODs could be attributed to the redox reaction between Hg^{2+} and L-AA. It is well known that the diol group of L-AA is oxidized to an 1,2-diketo group of the dehydroascorbic acid (DHAA) along with the reduction of the metal.[48] In this case, the Hg^{2+} should reduce to Hg^0 as proposed by Zheng.[49] Hg(0) has much lower ability to chelate NGODs, and the PL of NGODs can be partly restored (≈70%). All of these results indicated that the NGODs/AA could develop an effective fluorescence "on-off-on" sensor for the detection of Hg^{2+}. By the way, the addition of L-Cys to the system-containing NGODs−Hg^{2+} (quenched state) reveals that the relative emission intensity will be restored being close to that observed for NGODs in almost 90% (Figure 6b). This behavior has been observed in related systems and has been attributed to the high affinity of Hg^{2+} for the thiol group,[50]

DOI: 10.1021/acsomega.9b00858
ACS Omega 2019, 4, 10702−10713

Scheme 1. Schematic Illustration of the Proposed Mechanism: Hg^{2+} Detection and PL Recovery Using AA and Cystine (Upper Part of the Schematic) and Au^{3+} Detection Using L-Cys (Bottom Part of the Schematic)

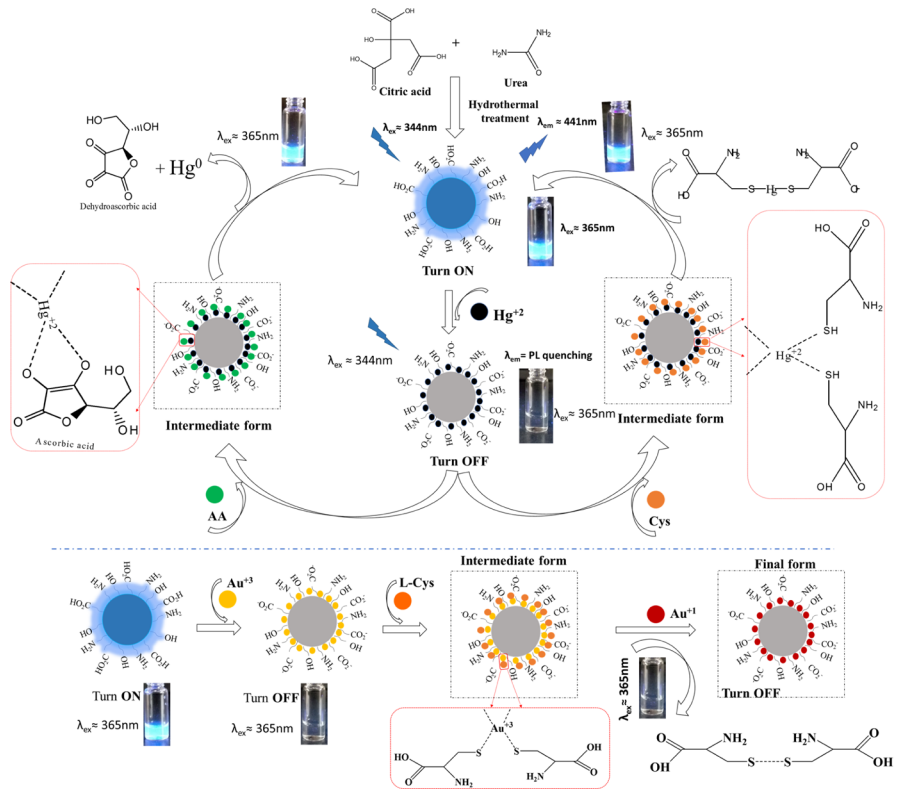

which favors the formation of the L-Cys−Hg^{2+} complex as described by Zheng[49] and showed at Figure 8. Thus, L-cysteine separates the metal ion from the hydrophilic groups on the surface of NGODs recovering the fluorescence. The PL signal intensity recovery from NGODs−Hg^{2+}−L-Cys/L-AA complexes is found to be very close to the original NGODs−L-Cys/L-AA PL intensity.

Although the turn-off mechanism is shown by both the metal ions (Scheme 1), that is, Hg^{2+} and Au^{3+}, the recovery of the PL (i.e., turn-off-on) using L-Cys and L-AA is only observed in the case of Hg^{2+}. The absence of PL recovery (or reversibility) after its annihilation in the presence of Au^{3+} could be attributed to the strong characteristic bonding between the carboxylate anions and Au^{+} ions. Upon the addition of L-AA or L-Cys to the NGODs−Au^{3+} system, a redox reaction takes place, that is, transformation of Au^{3+} ion into Au^{+} ion (reduction) accompanied with a simultaneous oxidation of L-AA to DHAA as schematized in the bottom part of Scheme 1. Additionally, L-Cys can also be oxidized to disulfur derivative (R−S−S−R). The Au^{+} ion has been reported to form stable complexes with carboxylate ions;[44] thus, Au^{+} ions are not removed from the surface of NGODs, and their presence at the periphery inhibits the PL recovery (remains off).

As the variation in the order of L-Cys/L-AA and Hg^{2+} addition in the NGOD luminescent probe system is found to significantly influence the resultant PL signal, Figure 6b shows the effect of its addition order at 3 different concentrations of L-Cys/L-AA, for a fixed concentration (250 μM) of Hg^{2+}. Although the PL signal recovery in the NGODs−Hg^{2+} system is attained by both the analytes L-Cys (blue bar) and L-AA (black bar), after the addition of Hg^{2+} in NGODs−L-Cys and NGODs−L-AA systems (i.e., reversing the order of addition in NGODs), Figure 6b clearly shows the appearance of the turn-on-on signal for NGODs−L-Cys and turn-on-off signal for L-AA (red bar), as the PL signal is retained even after the addition of Hg^{2+} in NGODs−L-Cys (bluish-green bar), which is on contrary to the case of NGODs−L-AA, where the signal drops (red bar) to less than 50% (below the green line).

Hence, after the annihilation of NGODs' PL through Hg^{2+}, recovering the PL through L-AA reveals the possibility of having a reusable optical sensor (testing through repetitive additions demonstrated in the following section). The recovery of PL intensity in NGODs−Hg^{2+}−L-Cys and NGODs−Hg^{2+}−L-AA complexes, tested for 3 different concentrations, corresponds to around 90 and 70%, respectively, revealing the independence of the recovered signal with respect to L-Cys/L-AA concentration. The detailed real-time PL measurements were carried out to know the time taken to complete the reaction from turn-off state to turn-on state (and viceversa) at different concentrations of L-Cys/L-AA (Figures S4−S6), revealing the difference in the reaction time for L-Cys and L-AA. Similarly, several citrus fruits tested for the recovery of PL signal intensity and the analysis graphs of concentration-dependent reduction of Hg^{2+} to Hg^{0} are presented in Figure 7 (PL spectra are presented in Figure S7). Already reported works related to PL recovery by L-Cys and L-AA are shown in Supporting Information Figures S8 and S9.

To further test whether our NGODs could be used in a real environment, the utilization of NGODs as a fluorescent probe to detect Hg^{2+} ions in tap water (TW) was examined with the water from three different places within Cuernavaca, Morelos, Mexico. Three types of TW were named TW1, TW2, and

DOI: 10.1021/acsomega.9b00858
ACS Omega 2019, 4, 10702−10713

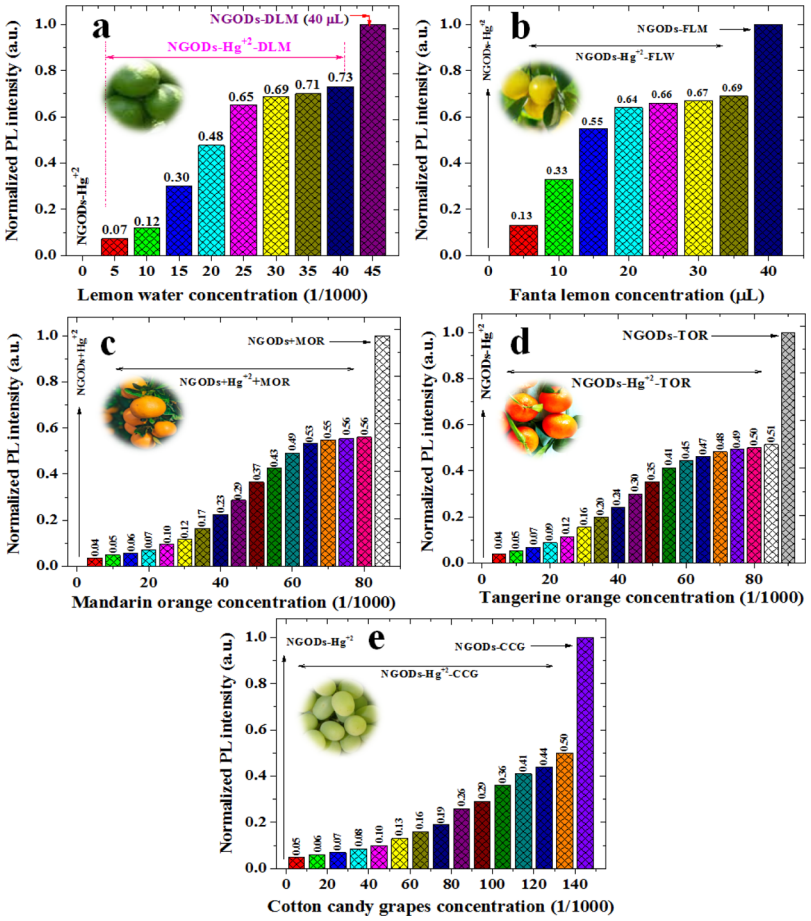

Figure 7. Comparison of sustainable PL recovery from Hg^{2+} detection: PL intensity ratio before and after the addition of different concentrations of various citrus fruits: (a) green lemon, (b) fanta lemon, (c) mandarin orange, (d) tangerine orange, and (e) cotton candy grapes. The citrus fruit juice was filtered using a filter paper and then diluted to 1/100 times with respect to the original concentration.

TW3. Similar to the results with deionized water, decline/quenching and recovery of emission intensity at 441 nm was observed after adding Hg^{2+} ions into NGOD-added TW (formation of NGODs−Hg^{2+} complex) followed by the addition of the L-AA to NGODs−Hg^{2+} complex (Figures S10 and S11). The values of F/F_0 versus the concentrations of Hg^{2+} ions detection are plotted in Figure S9d. Therefore, in spite of the interference from various minerals and contaminants existing in TW samples, the NGODs could still exhibit sensitive detections as well as recovery of fluorescence response toward the Hg^{2+} ions, suggesting that the as-prepared NGODs are capable of detecting and recovering the fluorescence from Hg^{2+} ions in a practical environment system.

The above observations open the possibility to use the proposed system for designing the mimic devices using basic logic gates (NOT and OR).

Basic Idea of Logic Gates Applied to the Optical Hg^{2+} Sensing System. The basic logic gates (NOT and OR gates) fabricated in this work use the characteristic PL emission response at 441 nm (at λ_{ex} = 344 nm) of the NGOD probe, upon the addition of Hg^{2+} ions (quenching) and L-Cys/L-AA (recovery) as chemical inputs[32] and the recorded variation in the PL emission as the output signal. Hence, in the present system, the output signal symbolizes an "off" state (with a Boolean arithmetic value of "0"), when the value of the PL emission intensity from NGODs is less than 50% and considered as an "on" state (with a Boolean arithmetic value of "1") when the emission is more than 50%.

Figure 8a−c shows the basic design of the two-input logic operation system using NGODs, which can operate as two different kinds of gates, depending on the metal ions and analytes (Hg^{2+}/Au^{3+}, L-Cys/L-AA), used as chemical inputs. Boolean expressions 0/1 were treated as gate inputs with/without the presence of Hg^{2+}. As specified previously, the difference in the emission intensities of NGODs (at peak wavelength 441 nm) was choosen as the output signal for analyzing on and off states of the system. The presence of the metal ion Hg^{2+}/Au^{3+} as an input in the absence of its counteranion L-Cys/L-AA represents the system expressed as the NOT gate (input A in Figure 8a), considered as one of the simplest logic gates. Corresponding truth table is shown as Figure 8b, where "0/1" in the input represents absence/presence of Hg^{2+} in the probe solution (NGODs), results in an output "1/0" representing the retention/quenching of the PL signal. Figure 8c shows the truth table corresponding to the formation of the OR gate, where one of the inputs is the output from the NOT gate (a system with/without Hg^{2+}) and the other is the analyte (L-Cys/L-AA) added to regain the PL signal. Hence, different chemical inputs can lead to the formation of four possible input string combinations: (i) (0/0), representing the presence of Hg^{2+} and absence of PL recovering analyte; (ii) (0/1), representing the presence of Hg^{2+} and PL recovering analyte; (iii) (1/0), representing the

DOI: 10.1021/acsomega.9b00858
ACS Omega 2019, 4, 10702−10713

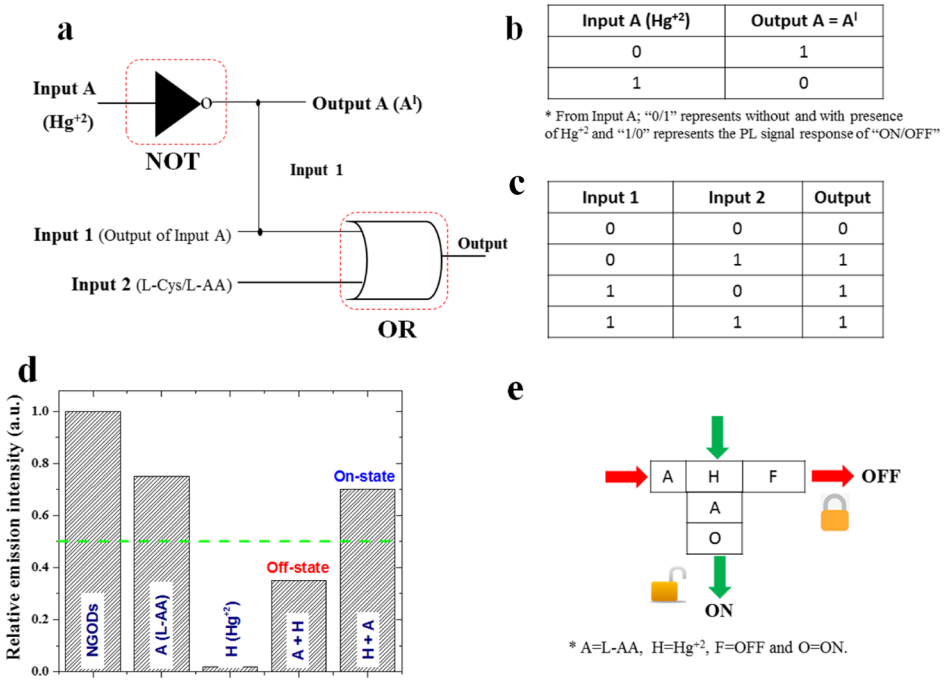

Figure 8. (a) Schematic representation of logic functions of NGODs with two chemical inputs Hg^{2+} and L-Cys/L-AA and (b) truth table for input A and output A (A^I) with its corresponding digital input and output signals representing NOT gate, and (c) truth table for input 1 (from the output of input A) and input 2 (L-Cys/L-AA) strings with its corresponding digital input and output signals representing OR gate, respectively. As conventionally accepted notations, the 0/OFF state represents no luminescence and 1 represents luminescence. (d) Bar diagram representing the change in the emission intensity of NGODs (chemical inputs were represented as A = L-AA; H = Hg^{2+}; F = off state and O = on state, respectively) and (e) schematic representation of a KSL model using NGODs as the molecular fluorescence system.

absence of Hg^{2+} and presence of PL recovering analyte; and (iv) (1/1), representing the absence of Hg^{2+} and presence of PL recovering analyte. Corresponding simulation results are presented in Supporting Information Figures S12 and S13.

The annhilation of NGODs' FL intensity due to the formation of the NGODs−Hg^{2+} complex, coincide with the NOT gate, that is, off state. Upon addition of L-Cys/L-AA (input 2 in the OR gate), the PL intensity was recovered, with almost 90 and 70% with L-Cys and L-AA, respectively. Thus, an OR gate has been constructed using Hg^{2+} and L-Cys/L-AA as input 1 and input 2, respectively. The presence of "turn-on state" in either one or both inputs (input 1 and input 2 in the OR gate) in the system is expressed as a turn-on state in the output. This clearly confirms that the decreased emission intensity in NGODs−Hg^{2+} is recovered by the NGODs−Hg^{2+}−L-Cys/L-AA complex formation. Thus, for future applications the proposed NGOD probes can possibly be used as molecular/chemical logic gates for the identification of Hg^{2+} in the real contaminated water samples through PL switching pattern and the use of fruit juices as recovering agents can be a step towards sustainable approach.

Security Lock-Type Mimic Device or Functioning of Molecular Logic Gates. The molecular/chemical computing (keypad lock) system, as a modern strategy for information security, has been proposed/utilized for restricted data applications.[32] In the present work, we have tested the possible incorporation of switching behavior idea (used in electronic security devices) in the present NGOD-Hg^{+2} ± l-AA system (Figure 8d,e). The PL emission signal difference represented in the form of a keypad security lock (KSL) system is shown inFigure 8e. For using NGODs as a probe in a security keypad sensing device for Hg^{2+}, the PL probe (NGODs) was exposed to the molecular/chemical inputs (Hg^{2+}, L-AA) (NGODs−Hg^{2+}, NGODs−L-AA). The hydroxyl groups present in L-AA will reduce Hg^{2+} to Hg^0, resulting in desorption of Hg^{2+} from the NGOD surface, leading to the off-on behavior. Thus, although operating, if we add L-AA to the system containing NGODs−Hg^{2+} (quenched state), the relative emission intensity will recover to around 69 ± 2% (with respect to the NGODs−L-AA complex system), which implies a turn-on state, whereas if we added Hg^{2+} to the system containing NGODs−L-AA (with the PL signal), the luminescence decreases to almost 40%, which denotes the turn-off state. Thus, changing the order of signal inputs, change in the output signals (PL intensity), enables the usage of the probe (NGODs) in designing a molecular/chemical keypad lock system. The lock can be removed (i.e., changing to the turn-on state; Figure S9e vertical column; H−A−O representing Hg^{2+} followed by AA resulting in the on state) using the order of inputs as NGODs → Hg^{2+} → L-AA, whereas we can lock again (i.e., change to turn-off state; Figure 8e horizontal column; A−H−F representing AA followed by Hg^{2+} resulting in off state) the device using the order of inputs NGODs → L-AA → Hg^{2+}.

In other words, in the crossword puzzles representing security lock devices (shown in Figure 8e), the analytes (Hg^{2+} and l-AA) used in the present case as chemical input signals, were named H and A (for Hg^{2+} and L-AA, respectively), and existence of PL signal (>70%) was interpreted as the output signal. The symbols O and F represent on and off states, respectively. Although executing the password, pressing H followed by A, the emission output will turn the switch on (O), (turn-on state), pressing A succeeded by H will cause turn the switch off (F) (turn-off stateFigure 8d). Thus, the password

DOI: 10.1021/acsomega.9b00858
ACS Omega 2019, 4, 10702−10713

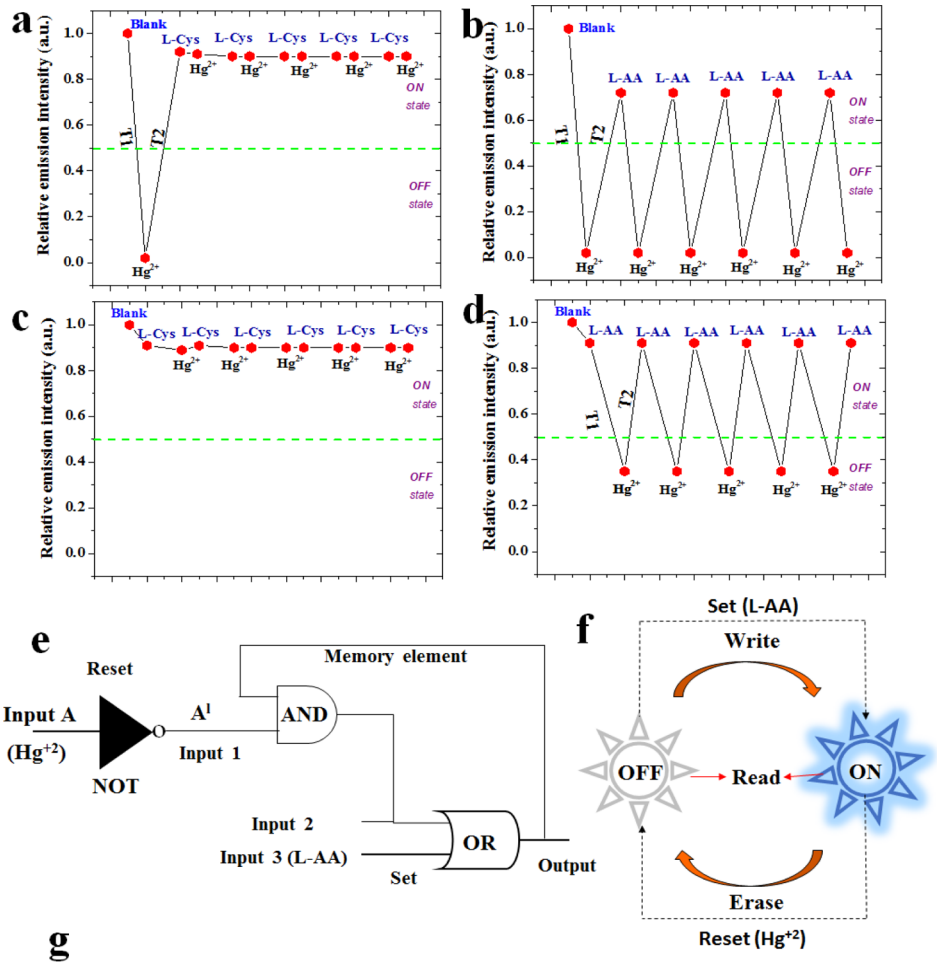

g

Input A	Reset (Output of A) Input 1	Memory element	Input 2 (Output of input 1)	Set Input 3 (L-AA)	Output
0	1	0	0	0	0
1	0	0	0	1	1
0	1	1	1	0	1
1	0	1	0	1	1

Figure 9. Reversibility of NGOD probe with the alternate addition of (a) Hg^{2+} and L-Cys, (b) Hg^{2+} and L-AA, (c) L-Cys and Hg^{2+}, (d) L-AA and Hg^{2+} (the concentration of Hg^{2+}, L-Cys, and L-AA was maintained at 250 μM), and (e) feedback loops with write−read−erase−read function, (f) sequential logic circuit of the memory unit, and (g) truth table of the memory unit. In Figures (a)−(d), X-axis represents sequence of addition.

AHF will lock the device, whereas the password HAO opens the lock without fail. The corresponding simulation results are presented in Figure S14.

Mimicking Memory Devices. Due to the observed switching behaviour (the reversibility upon alternating the addition of l-Cys/l-AA and Hg^{+2}), the proposed structure/setup has been analyzed for its possible usage as memory element in logic circuit for processing information at molecular-level (Figure 9).

After the addition of L-Cys/L-AA to the probe NGODs−Hg^{2+} complex, different cycles of real-time PL measurements reveal time-dependent change in the PL signal intensity from the sample mixture containing NGODs−Hg^{2+}−L-Cys complex (Figure 9a,b) and NGODs-Hg^{2+}-l-AA (Figure 9c,d). As discussed earlier (ref to Figure 6b), the recovery of PL signal intensity was observed. Although after the first addition of L-Cys into the NGODs−Hg^{2+} complex (Figure 9a), there was a significant change in the PL signal intensity, subsequent additions made no change in PL intensity signal, indicating that the NGODs−Hg^{2+}−L-Cys complex system is not suitable for the reuseable memory device at this molar equivalent with respect to Hg^{2+}. However, in the case L-AA, there was a noticeable change according to the additions of Hg^{2+} in the probe system, which means that the NGODs−Hg^{2+}−L-AA complex can be used as a reuseable memory device (Figure 9b).

The addition of L-Cys/L-AA to the probe NGOD solution (before the addition of Hg^{2+}) reveals no significant change in the signal intensity (Figure 9c and d). In the real-time PL measurements from the sample mixture containing the NGODs−L-Cys−Hg^{2+} complex (Figure 9c) (even after 10 min) no significant change in the signal intensity is observed whereas an immediate drastic decrement is revealed in the FL intensity for the NGODs−L-AA−Hg^{2+} complex (Figure 9d).

DOI: 10.1021/acsomega.9b00858
ACS Omega 2019, 4, 10702−10713

These results confirm the strength of NGODs−L-Cys complex as compared to NGODs−L-AA complex where the former retains the PL and prevents the charge transfer even after the incorporation of Hg^{2+}. As per the PL analysis (Figure S4), after the addition of Hg^{2+} to the NGODs−L-Cys complex, there is slight decrement (i.e., ≈2% as compared with the original signal from the NGODs−L-Cys complex) in the PL intensity; after the alternative addition of L-Cys and Hg^{2+} to the above system, there is no observable change in the PL peak intensity; hence, it is acting as a turn-on-on sensor. In the case of the NGODs−L-AA−Hg^{2+} complex, there is around 60% decrement (from around 90% of the NGODs−L-AA complex) in the PL intensity, demonstrating the formation of the turn-on-off Hg^{2+} sensor in the case of the NGODs−L-AA−Hg^{2+} complex.

Furthermore, similar to the logic circuits (implementation of Boolean functions to store the information) demonstrated before, where they can be controlled through one or more logic inputs (connected through a response loop), for obtaining one output (identified as memory element for the given inputs),[32] in the present case, for imitating the behavior of a memory element, chemical input Hg^{2+} (input 1 is the output of NOT gate) is used as reset and L-Cys/L-AA (input 3) as set (Figure 9e,f). The operation of Figure 9e is almost similar to that of Figure 8a, except the use of memory element as an input to the AND gate. The input of memory element is the previous output of the circuit (i.e., the initial input to the memory element is "0" representing an "off" state). Hence, four possible input string combinations for set are (0/0), (0/1), (1/0), and (1/1). One of the inputs (input 2; from Figure 9e,g) of set depends on the input 1 and memory element; another input in set (input 3) strings 0/1 represents the absence and presence of L-AA into the system.

Figure 9f shows schematic representation of the "Erase−Read−Write−Read" nature of the present system i.e., as a first step the addition of Hg^{2+} to NGODs as a probe shows the quenching effect in the PL signal intensity, which shows erase nature of the system. As the second step, the addition of L-AA to the NGODs−Hg^{2+} complex shows the PL signal recovery, which signifies "write" nature of the system. In between these erase and write nature, it shows "read" nature representing the information that was memorized, showing a continuous "erase−read−write−read" cycle with alternative additions of Hg^{2+} and L-AA. The corresponding simulations were done and are presented in Supporting Information (Figures S15 and S16). Hence, the proposed system can possibly be used as a molecular microprocessor, that is, as a possible substitute for the conventional memory element in ICs (integrated circuits).

CONCLUSIONS

Sustainable reusable mercury sensing nanoprobes, synthesized via hydrothermal treatment using citric acid as a carbon precursor and urea as a nitrogen dopant, reveal the characteristic excitation wavelength independent emission at 441 nm. Sharp XRD peak centered at 11.31°, confirming the formation of NGODs, is attributed to the graphitic structure with an interlayer spacing (001) of 0.78 nm. Highly fluorescent NGOD-based sensing probes are found to be selective and sensitive for the detection of enzyme-free H_2O_2 and label-free Hg^{2+}/Au^{3+} ions with the LOD of about 0.20, 0.20, and 0.25 μM, respectively. The sustainable PL signal recovery of almost 70%, after the detection of Hg^{2+} ions, is observed using AA and naturally available citrus fruits. As compared to the already reported PL recovery of the NGODs−Hg^{2+} system through L-cysteine, where the PL signal recovers ≈90% using double the molar equivalents with respect to Hg^{2+}, 70% signal recovery through AA is achieved with equivalent proportions of the corresponding metal ion. The fluorescent switching mechanism has been attributed to the reduction of Hg^{2+} to Hg^0 followed by its segregation from the sensing probe and hence contributing to the recovery of the PL signal. In the case of Au^{3+}, the absence of PL recovery (or reversibility) has been attributed to the strong characteristic bonding between the carboxylate anions and Au^+ ions, formed because of the redox reaction resulting in the reduction of Au^{3+} to Au^+, accompanied with a simultaneous oxidation of L-AA and L-Cys to DHAA and disulfur derivative (R−S−S−R), respectively. The proposed Hg(II) sensor was also tested and verified on real water samples. Furthermore, the NGOD-based multiple logic gates were designed, and their capacity of mimicking a memory device at the molecular level with chemical inputs of Hg^{2+} ion and L-Cys/L-AA has been demonstrated. Such NGODs have possible applications as molecular microprocessors, an alternative for the traditional memory element in integrated logic circuits.

MATERIALS AND METHODS

Synthesis of NGODs. NGODs were prepared by the hydrothermal method, using citric acid (0.2 g) and urea (0.38 g) (Sigma-Aldrich) in wt. ratio of around 1:2, in 50 mL of deionized water (18.2 MΩ cm), stirred (15 min), and kept in a Teflon autoclave at 180 °C for 60 min. NGODs were stored at RT for further use.

Characterization. Optical properties, including UV−visible and fluorescence spectra, of as-synthesized NGODs were monitored by dual beam PerkinElmer LAMBDA 950 and Cary Eclipse fluorescence spectrophotometer, respectively. JEOL JEM-ARM200F was used to carry out TEM measurements for determining the particle size distribution of the synthesized NGODs. A 100 mesh Cu grid with a lacey carbon film was used for the sample preparation by drop-casting of NGODs and subsequent evaporation under ambient conditions. A Bruker D8 X-ray diffractometer with Cu Kα radiation (λ = 1.5406 Å) was used for measuring the diffraction pattern. For surface-sensitive quantitative analysis, Al Kα radiation photon energy (1486.6 ± 0.2 eV) from an ESCA Ulvac-PHI 1600 photoelectron spectrometer was used. The FTIR spectra of NGODs in the aqueous medium were measured using a Varian 660-IR FTIR spectrophotometer. Electronic circuit modeling was executed using Proteus 8 Professional.

Selectivity and Sensitivity Procedure. To determine the relative selectivity of NGODs toward Hg^{2+}, interference studies were conducted on some common heavy metal ions in the presence of NGODs (5 μL of NGOD's stock solution in 400 μL of 250 μM metal ion solution). The PL response of NGODs was examined under identical conditions/concentrations of 4 mg/mL NGOD solution with 250 μM Fe^{2+}, Cu^{3+}, Co^{2+}, Ni^{2+}, Hg^{2+}, Ag^+, Mn^{2+}, Mg^{2+}, Zn^{2+} ions, arsenic, L-Cys, L-AA, L-glutamic acid, glucose, fructose, sucrose, and 300 μM Au^{3+}. All of the heavy metals and analytes were of analytical grade and used as received from Sigma-Aldrich. Among these, Hg^{2+} and Au^{3+} show a significant decrease in PL intensity with increasing concentration. Similar procedure was used for the detection of H_2O_2. Then, the PL spectra measured for recording the PL signal intensity.

DOI: 10.1021/acsomega.9b00858
ACS Omega 2019, 4, 10702−10713

■ ASSOCIATED CONTENT

Supporting Information

The Supporting Information is available free of charge on the ACS Publications website at DOI: 10.1021/acsomega.9b00858.

XPS full survey scan and FTIR of as-prepared NGODs; PL spectroscopy analysis of Ag^{+}, Mn^{2+}, Mg^{2+}, and Zn^{2+}; effect of variation in the order of addition of L-Cys and Hg^{2+} at three different concentrations of L-Cys; effect of variation in the order of addition of L-AA and Hg^{2+} at three different concentrations of L-AA; data analysis of Figures S3 and S4 representing time taken in PL signal recovery with L-Cys and L-AA and quenching during Hg^{2+} detection; PL response of NGODs + Hg^{2+} in different dilutions of 5 citrus fruit juice (lemon/fanta lemon/mandarina orange/tangerine orange/cotton candy grape); schematically represented outcome of similar works related to PL signal recovery using L-Cys and anion HS^{-}; schematically represented outcome of similar works related to PL signal recovery (quenching from Cr^{6+} and Fe^{3+}) using L-AA; optical response of NGODs from Hg^{2+}-spiked real TW collected from three different places; regained PL signal (%) from Hg^{2+}-spiked TW sample from 3 different locations at 3 different concentrations of L-AA; NGODs−Hg^{2+} complex representing NOT gate; and electronic circuit simulations corresponding to Figure 8a (NOT and OR gate), Figure 8e, Figure 9e, and Figure 9f (PDF)

■ AUTHOR INFORMATION

Corresponding Author

*E-mail: vagarwal@uaem.mx.

ORCID

Vivechana Agarwal: 0000-0003-2168-853X

Author Contributions

N.K.R.B. and V.A. contributed equally in planning and execution of the project. V.B. contributed in the sensing mechanism part. All of the authors commented on the manuscript during its preparation.

Notes

The authors declare no competing financial interest.

■ ACKNOWLEDGMENTS

Special gratitude is expressed to Kiran Kumar Anna (Centro de Investigación y de Estudios Avanzados del IPN, Unidad Querétaro Apdo, 76001 Querétaro, México) for his help in performing the TEM and XPS measurements.

■ REFERENCES

(1) Li, Y.; Hu, Y.; Zhao, Y.; Shi, G.; Deng, L.; Hou, Y.; Qu, L. An electrochemical avenue to green-luminescent graphene quantum dots as potential electron-acceptors for photovoltaics. *Adv. Mater.* **2011**, *23*, 776−780.

(2) Yan, X.; Cui, X.; Li, L.-s. Synthesis of Large, Stable Colloidal Graphene Quantum Dots with Tunable Size. *J. Am. Chem. Soc.* **2010**, *132*, 5944−5945.

(3) Li, L.-L.; Ji, J.; Fei, R.; Wang, C.-Z.; Lu, Q.; Zhang, J.-R.; Jiang, L.-P.; Zhu, J.-J. A Facile Microwave Avenue to Electro-chemiluminescent Two-Color Graphene Quantum Dots. *Adv. Funct. Mater.* **2012**, *22*, 2971−2979.

(4) Tang, L.; Ji, R.; Cao, X.; Lin, J.; Jiang, H.; Li, X.; Teng, K. S.; Luk, C. M.; Zeng, S.; Hao, J.; Lau, S. P. Deep ultraviolet photoluminescence of water-soluble self-passivated graphene quantum dots. *ACS Nano* **2012**, *6*, 5102−5110.

(5) Zhu, S.; Zhang, J.; Qiao, C.; Tang, S.; Li, Y.; Yuan, W.; Li, B.; Tian, L.; Liu, F.; Hu, R.; Gao, H.; Wei, H.; Zhang, H.; Sun, H.; Yang, B. Strongly green-photoluminescent graphene quantum dots for bioimaging applications. *Chem. Commun.* **2011**, *47*, 6858−6860.

(6) Lin, L.; Zhang, S. Creating high yield water soluble luminescent graphene quantum dots via exfoliating and disintegrating carbon nanotubes and graphite flakes. *Chem. Commun.* **2012**, *48*, 10177−10179.

(7) Zhang, Y.; Zhao, H.; Wu, Z.; Xue, Y.; Zhang, X.; He, Y.; Li, X.; Yuan, Z. A novel graphene-DNA biosensor for selective detection of mercury ions. *Biosens. Bioelectron.* **2013**, *48*, 180−187.

(8) Cai, F.; Zhu, Q.; Zhao, K.; Deng, A.; Li, J. Multiple Signal Amplified Electro Chemiluminescent Immunoassay for Hg2+ Using Graphene-Coupled Quantum Dots and Gold Nanoparticles-Labeled Horseradish Peroxidase. *Environ. Sci. Technol.* **2015**, *49*, 5013−5020.

(9) Jiang, C.; Liu, R.; Han, G.; Zhang, Z. A chemically reactive Raman probe for ultra-sensitively monitoring and imaging the in vivo generation of femtomolar oxidative species as induced by anti-tumor drugs in living cells. *Chem. Commun.* **2013**, *49*, 6647−6649.

(10) Zhang, R.; Zhao, J.; Han, G.; Liu, Z.; Liu, C.; Zhang, C.; Liu, B.; Jiang, C.; Liu, R.; Zhao, T.; Han, M.-Y.; Zhang, Z. Real-Time Discrimination and Versatile Profiling of Spontaneous Reactive Oxygen Species in Living Organisms with a Single Fluorescent Probe. *J. Am. Chem. Soc.* **2016**, *138*, 3769−3778.

(11) Long, Z.; Fang, D.-C.; Ren, H.; Ouyang, J.; He, L.; Na, N. Excited Oxidized-Carbon Nanodots Induced by Ozone from Low-Temperature Plasma to Initiate Strong Chemiluminescence for Fast Discrimination of Metal Ions. *Anal. Chem.* **2016**, *88*, 7660−7666.

(12) Zhang, K.; Zhou, H.; Mei, Q.; Wang, S.; Guan, G.; Liu, R.; Zhang, J.; Zhang, Z. Instant visual detection of trinitrotoluene particulates on various surfaces by ratio metric fluorescence of dual-emission quantum dots hybrid. *J. Am. Chem. Soc.* **2011**, *133*, 8424−8427.

(13) Noyori, R.; Masao, A.; Kazuhiko, S. Green oxidation with aqueous hydrogen peroxide. *Chem. Commun.* **2003**, 1977−1986.

(14) Yang, X.; Ouyang, Y.; Wu, F.; Hu, Y.; Ji, Y.; Wu, Z. Size controllable preparation of gold nanoparticles loading on graphene sheets@ceriumoxide nanocomposites modified gold electrode for nonenzymatic hydrogen peroxide detection. *Sens. Actuators, B* **2017**, *238*, 40−47.

(15) Wang, H.; Wang, H.; Li, T.; Ma, J.; Li, K.; Zuo, X. Silver nanoparticles selectively deposited on graphene-colloidal carbon sphere composites and their application for hydrogen peroxide sensing. *Sens. Actuators, B* **2017**, *239*, 1205−1212.

(16) Ensafi, A. A.; Rezaloo, F.; Rezaei, B. Electrochemical sensor based on porous silicon/silver nanocomposite for the determination of hydrogen peroxide. *Sens. Actuators, B* **2016**, *231*, 239−244.

(17) Akhtar, N.; El-Safty, S.; Khairy, M. Simple and Sensitive Electrochemical Sensor-Based Three-Dimensional Porous Ni-Hemoglobin Composite Electrode. *Chemosensors* **2014**, *2*, 235−250.

(18) Sunil, K.; Narayana, B. Spectrophotometric determination of hydrogen peroxide in water and cream samples. *Bull. Environ. Contam. Toxicol.* **2008**, *81*, 422−426.

(19) Lei, W.; Dürkop, A.; Lin, Z.; Wu, M.; Wolfbeis, O. S. Detection of Hydrogen Peroxide in River Water via a Microplate Luminescence Assay with Time-Resolved ("Gated") Detection. *Microchim. Acta* **2003**, *143*, 269−274.

(20) Vašíček, O.; Papežíková, I.; Hyršl, P. Fluorimetric determination of hydrogen peroxide production by the haemocytes of the wax moth Galleria mellonella (Lepidoptera: Pyralidae). *Eur. J. Entomol.* **2011**, *108*, 481−485.

(21) Lu, W.; Qin, X.; Liu, S.; Chang, G.; Zhang, Y.; Luo, Y.; Asiri, A. M.; Al-Youbi, A. O.; Sun, X. Economical, Green Synthesis of Fluorescent Carbon Nanoparticles and Their Use as Probes for Sensitive and Selective Detection of Mercury (II) Ions. *Anal. Chem.* **2012**, *84*, 5351−5357.

DOI: 10.1021/acsomega.9b00858
ACS Omega 2019, 4, 10702−10713

(22) Chakraborty, D.; Sarkar, S.; Das, P. K. Blood Dots: Hemoglobin-Derived Carbon Dots as Hydrogen Peroxide Sensors and Pro-Drug Activators. *ACS Sustainable Chem. Eng.* **2018**, *6*, 4661−4670.
(23) Bhunia, S. K.; Dolai, S.; Sun, H.; Jelinek, R. "On/off/on" hydrogen-peroxide sensor with hemoglobin-functionalized carbon dots. *Sens. Actuators, B* **2018**, *270*, 223−230.
(24) Zhang, Y.; Wu, C.; Zhou, X.; Wu, X.; Yang, Y.; Wu, H.; Guo, S.; Zhang, J. Graphene quantum dots/gold electrode and its application in living cell H_2O_2 detection. *Nanoscale* **2013**, *5*, 1816−1819.
(25) Wang, W.-W.; Yu, Q.; Shao-Peng, Z.; Jia-Wei, L.; Xiao-Quan, L.; Xiu-Hui, L. A Hydrogen Peroxide Sensor Based on Pt@Au Nanoparticles Loading to Polyethyleneimine Functionalized Carbon Nanotubes. *Chin. J. Anal. Chem.* **2014**, *42*, 835−841.
(26) Song, L.; Cui, Y.; Zhang, C.; Hu, Z.; Liu, X. Microwave-assisted facile synthesis of yellow fluorescent carbon dots from o-phenylenediamine for cell imaging and sensitive detection of Fe3+ and H2O2. *RSC Adv.* **2016**, *6*, 17704−17712.
(27) Wei, J.; Qiang, L.; Ren, J.; Ren, X.; Tang, F.; Meng, X. Fluorescence turn-off detection of hydrogen peroxide and glucose directly using carbon nanodots as probes. *Anal. Methods* **2014**, *6*, 1922−1927.
(28) Zhang, R.; Chen, W. Nitrogen-doped carbon quantum dots: Facile synthesis and application as a "turn-off" fluorescent probe for detection of Hg^{2+} ions. *Biosens. Bioelectron.* **2014**, *55*, 83−90.
(29) Wang, Y.; Kim, S.-H.; Feng, L. Highly luminescent N, S- Co-doped carbon dots and their direct use as mercury (II) sensor. *Anal. Chim. Acta* **2015**, *890*, 134−142.
(30) Yan, F.; Shi, D.; Zheng, T.; Yun, K.; Zhou, X.; Chen, L. Carbon dots as nanosensor for sensitive and selective detection of Hg^{2+} and l-cysteine by means of fluorescence "Off−On" switching. *Sens. Actuators, B* **2016**, *224*, 926−935.
(31) Zhang, Y.; Cui, P.; Zhang, F.; Feng, X.; Wang, Y.; Yang, Y.; Liu, X. Fluorescent probes for "off−on" highly sensitive detection of Hg^{2+} and L-cysteine based on nitrogen-doped carbon dots. *Talanta* **2016**, *152*, 288−300.
(32) Vandarkuzhali, S. A. A.; Natarajan, S.; Jeyabalan, S.; Sivaraman, G.; Singaravadivel, S.; Muthusubramanian, S.; Viswanathan, B. Pineapple Peel-Derived Carbon Dots: Applications as Sensor, Molecular Keypad Lock, and Memory Device. *ACS Omega* **2018**, *3*, 12584−12592.
(33) Zheng, M.; Xie, Z.; Qu, D.; Li, D.; Du, P.; Jing, X.; Sun, Z. On−Off−On Fluorescent Carbon Dot Nanosensor for Recognition of Chromium (VI) and Ascorbic Acid Based on the Inner Filter Effect. *ACS Appl. Mater. Interfaces* **2013**, *5*, 13242−13247.
(34) Gong, J.; Lu, X.; An, X. Carbon dots as fluorescent off−on nanosensors for ascorbic acid detection. *RSC Adv.* **2015**, *5*, 8533−8536.
(35) Rong, M.; Lin, L.; Song, X.; Wang, Y.; Zhong, Y.; Yan, J.; Feng, Y.; Zeng, X.; Chen, X. Fluorescence sensing of chromium (VI) and ascorbic acid using graphitic carbon nitride nanosheets as a fluorescent "switch". *Biosens. Bioelectron.* **2015**, *68*, 210−217.
(36) Fong, J. F. Y.; Chin, S. F.; Ng, S. M. A unique "turn-on" fluorescence signalling strategy for highly specific detection of ascorbic acid using carbon dots as sensing probe. *Biosens. Bioelectron.* **2016**, *85*, 844−852.
(37) Luo, X.; Zhang, W.; Han, Y.; Chen, X.; Zhu, L.; Tang, W.; Wang, J.; Yue, T.; Li, Z. N,S co-doped carbon dots based fluorescent "on-off-on" sensor for determination of ascorbic acid in common fruits. *Food Chem.* **2018**, *258*, 214−221.
(38) Gu, J.; Hu, D.; Wang, W.; Zhang, Q.; Meng, Z.; Jia, X.; Xi, K. Carbon dot cluster as an efficient "off−on" fluorescent probe to detect Au(III) and glutathione. *Biosens. Bioelectron.* **2015**, *68*, 27−33.
(39) Liao, J.; Cheng, Z.; Zhou, L. Nitrogen-Doping Enhanced Fluorescent Carbon Dots: Green Synthesis and Their Applications for Bioimaging and Label-Free Detection of Au^{3+} Ions. *ACS Sustainable Chem. Eng.* **2016**, *4*, 3053−3061.
(40) Abraham, J.; Vasu, K. S.; Williams, C. D.; Gopinadhan, K.; Su, Y.; Cherian, C. T.; Dix, J.; Prestat, E.; Haigh, S. J.; Grigorieva, I. V.; Carbone, P.; Geim, A. K.; Nair, R. R. Tunable sieving of ions using graphene oxide membranes. *Nat. Nanotechnol.* **2017**, *12*, 546−550.
(41) Stobinski, L.; et al. Graphene oxide and reduced graphene and oxide studied by the XRD, TEM electron spectroscopy methods. *J. Electron Spectrosc. Relat. Phenom.* **2014**, *195*, 145−154.
(42) Moon, I. K.; Lee, J.; Ruoff, RS.; Lee, H. Reduced graphene oxide by chemical graphitization. *Nat. Commun.* **2010**, *1*, 73.
(43) Bagri, A.; Cecilia, M.; Muge, A.; Yves, JC.; Manish, C.; Vivek, B. S. Structural evolution during the reduction of chemically derived graphene oxide. *Nat. Chem.* **2010**, *2*, 581−587.
(44) Vandarkuzhali, S. A. A.; Jeyalakshmi, V.; Sivaraman, G.; Singaravadivel, S.; Krishnamurthy, K. R.; Viswanathan, B. Highly fluorescent carbon dots from Pseudo-stem of banana plant: Applications as nanosensor and bio-imaging agents. *Sens. Actuators, B* **2017**, *252*, 894−900.
(45) Zhang, R.; Chen, W. Nitrogen-doped carbon quantum dots: Facile synthesis and application as a "turn-off" fluorescent probe for detection of Hg^{2+} ions. *Biosens. Bioelectron.* **2014**, *55*, 83−90.
(46) Misra, A.; Srivastava, P.; Shahid, M. Fluorescent probe mimicking multiple logic gates and a molecular keypad lock upon interaction with Hg^{+2} and bovine serum albumin. *Analyst* **2012**, *137*, 3470−3478.
(47) Taylor, N. J.; Carty, A. J. Nature of Hg^{2+}-L-Cysteine Complexes Implicated in Mercury Biochemistry. *J. Am. Chem. Soc.* **1977**, *99*, 6143−6145.
(48) Luo, X.; Zhang, W.; Han, Y.; Chen, X.; Zhu, L.; Tang, W.; Wang, J.; Yue, T.; Li, Z. N, S co-doped carbon dots based fluorescent "on-off-on" sensor for determination of ascorbic acid in common fruits. *Food Chem.* **2018**, *258*, 214−221.
(49) Zheng, W.; Liang, L.; Gu, B. Mercury Reduction and Oxidation by Reduced Natural Organic Matter in Anoxic Environments. *Environ. Sci. Technol.* **2012**, *46*, 292−299.
(50) Tuchscherer, A.; Schaarschmidt, D.; Schulze, S.; Hietschold, M.; Lang, H. Gold nanoparticles generated by thermolysis of "all-in-one" gold(I) carboxylate complexes. *Dalton Trans.* **2012**, *41*, 2738−2746.

DOI: 10.1021/acsomega.9b00858
ACS Omega 2019, 4, 10702−10713